

Micromechanical Modelling of Multiple Fracture in Engineered Cementitious Composites

Andrea Spagnoli^{1,a}, En-Hua Yang^{2,b}, Victor C. Li^{2,c}

¹Department of Civil-Environmental Engineering and Architecture, University of Parma, Italy

² Department of Civil and Environmental Engineering, University of Michigan, MI, USA

^aspagnoli@unipr.it, ^behy@umich.edu, ^cvcli@umich.edu

Keywords: Cementitious composite; Fiber reinforced concrete; Micromechanics; Microstructure randomness; Tensile ductility.

Abstract. Engineered Cementitious Composites (ECC), a special class of high performance fiber reinforced cementitious composites, present, among other features, a superior tensile ductility which is the result of multiple cracking in the material. In the present paper, a micromechanical model is proposed to estimate the tensile strain capacity of ECC. The model takes into account the randomness in size and in spatial distribution of material flaws.

Introduction

Engineered Cementitious Composites (ECC), a special class of high performance fiber reinforced cementitious composites, have been developed to achieve specific composite performances which can be designed on the basis of the micromechanics of the material [1,2]. Under tensile loading, in contrast to normal concrete where a single unstable crack develops, an important characteristic of ECC is the development of multiple stable micro-cracks bridged by fibers. Consequently, tensile stress-strain curves of ECC exhibit a strain-hardening response with a superior ductility (ultimate strain up to 8%, with a certain degree of scattering), which is several hundred times that of normal concrete [3]. It has experimentally been observed that the tensile ductility of ECC is influenced by the number of stable micro-cracks developing before failure. A maximum ductility is reached for a so-called saturated cracking of the material (crack spacing in the saturated condition is directly correlated with fiber length, and crack width is of the order of a hundredth of a millimeter).

The multiple micro-cracking behavior of ECC is strongly dependent on the fiber crack bridging law, in relation to the so-called steady-state condition for crack propagation [4], and on the degree of heterogeneity in the material, in relation to the condition for crack initiation. Typically, crack initiation sites in ECC material are at material flaws, which are in the majority of cases voids (bubbles of entrapped air). Consequently, crack initiation behavior is influenced by the size and spatial distribution (which are both random in nature) of voids in the material [5,6].

Some theoretical models are available in the literature to describe the tensile behaviour of ECC (e.g. see [7,8]). However, the detail links between material microstructure and composite performance requires further clarification. In the present paper, a simple micromechanical model is proposed to predict the overall tensile stress-strain curves of ECC. The material is treated as a chain of reference volume elements where each element contains a material flaw. Conditions for crack initiation at the flaw surface and for steady-state crack propagation within the reference volume element are defined. The model takes into account the randomness in size and in spatial distribution of material flaws.

Description of the Micromechanical Model

Basic Assumptions. A two-dimensional model of a rectangular specimen made up with ECC under tensile loading is considered. The material, treated as a two phased composite material, is assumed to be composed of a matrix (mortar), having a homogeneous, isotropic and linear-elastic behavior, and of a number of circular voids (flaws). Spatial distribution and size (radius) of voids is random. (No randomness is considered at present for the mechanical properties of the matrix and of the fiber crack bridging law.) A schematic representation of the model (with dimensions $H \times W$) is reported in Fig. 1a.

The basic assumptions of the model are as follows:

- (i) the specimen is treated as a chain of reference volumes (RVEs), where each RVE contains a single void (see Fig. 1b);
- (ii) in each RVE, crack initiation occurs at the void surface;
- (iii) after crack initiation, propagation of a fully developed steady-state (SS) crack occurs in each RVE perpendicularly to the loading axis;
- (iv) interaction between void and cracks already developed in adjacent voids might occurs;
- (v) failure of the specimen occurs when the applied stress attains the peak stress of the fiber crack bridging law.

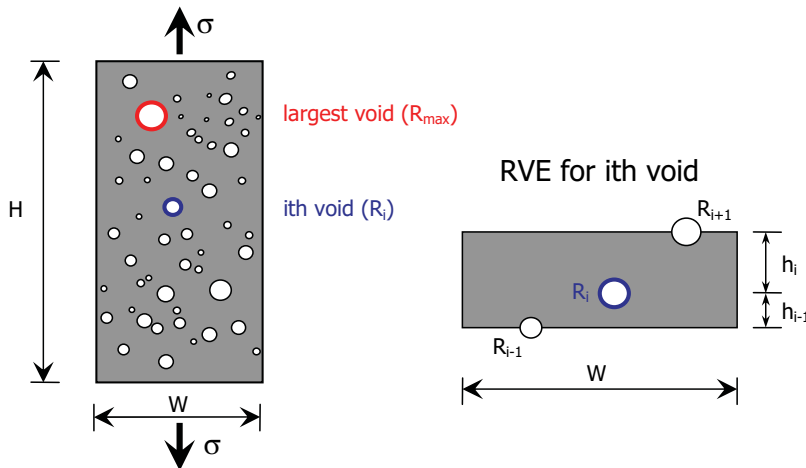


Figure 1. Schematic of the model.

Statistical Aspects. As is shown in Fig. 1b, the dimensions of the i th RVE are $(h_{i-1} + h_i) \times W$, where h_i is the distance along the loading axis between the centre of the i th void and that of the $(i+1)$ th void. The distribution of void radius R is assumed to be described by a given Probability Density Function (PDF), $p(R)$, where the radius R ranges from R_{min} to R_{max} . Now the number of voids with radius falling in the range R to $R+dR$ is given by

$$n(R) = \frac{f_{void}HW}{\pi R^2} p(R) \tag{1}$$

where f_{void} is the volume (area) fraction of voids. The number of voids, with radius R ranging from R_{min} to R_{max} , in the specimen of dimensions $H \times W$ is

$$N_{TOT} = \int_{R_{min}}^{R_{max}} n(R) dR \tag{2}$$

As has been mentioned above, the spatial distribution of voids is also random, but only their spatial distribution along the loading axis is relevant here for the present model. Therefore a given PDF of the void spacing along the loading axis, $p(h)$, with h ranging from 0 to H , is defined. It is assumed that such a PDF is uncorrelated with the PDF of void radius. The sole obvious condition which has to be met by the function $p(h)$ is

$$H = N_{TOT} \int_0^H p(h) h dh \tag{3}$$

The Analyses Procedure. The tensile load is applied in a step-by-step procedure under stress control. More precisely, following an event-to-event approach, the stress increment at each step causes the initiation and development of a new crack. The steps of the procedure are as follows:

- (i) Crack initiation at the largest void (calculation of a characteristic length of the initiated crack);
- (ii) Development of a SS crack in the RVE with the largest void;
- (iii) Crack initiation in the next most highly stressed void;
- (iv) Development of a SS crack in the next most highly stressed RVE.

Mechanics of Crack Initiation and Propagation. The initiation of the first crack at the void surface with the largest radius is assumed to be governed by the following criterion based on linear elastic fracture mechanics concepts. Accordingly, in the specimen submit to a tensile stress equal to the first cracking stress of the material a Mode I crack with a characteristic length a_0 emanates from the largest void. The length a_0 of such a crack can be determined by the following expression for the Stress Intensity Factor (SIF) [9]

$$\sqrt{EJ_{TIP}} = F(a_0/R_{max}) f_{cr} \sqrt{\pi a_0} \tag{4}$$

where J_{TIP} = fracture energy of the matrix; E = Young modulus of the matrix; f_{cr} = first cracking stress; F = geometric/loading factor. The first cracking stress of ECC material has been observed to be dependent, among other factors, on the largest size of flaws contained in the specimen [6]. It is worth noticing that, as is shown by the adopted SIF of Eq. 4, the crack bridging effect of fibers is neglected in the crack initiation stage (consider that the crack length a_0 is small enough not to activate the crack bridging action of fibers).

As the applied stress increases, further cracks initiates at the other voids. The corresponding matrix cracking stress σ_i is obtained by assuming that the length of the crack emanating from each void remains constant and equal to a_0 , namely

$$\sigma_i = \frac{\sqrt{EJ_{TIP}}}{F(a_0/R_i) \sqrt{\pi a_0}} \tag{5}$$

Note that according to the adopted criterion for crack initiation the experimentally-observed dependence of the matrix cracking stresses on the void size is taken into account [7].

Under crack initiation stress σ_i , a SS crack (emanating perpendicularly to the loading axis from the i th void) of length W instantly develops throughout the material (Fig. 2). The SS crack opening

displacement δ_i (note that SS cracks are characterized by a flat profile [4]) is that corresponding to the crack initiation stress σ_i according to the adopted fiber crack bridging law $\sigma(\delta)$ (e.g. see insert in Fig. 2). The condition for SS cracking is [4]

$$\sigma_i \delta_i - \int_0^{\delta_i} \sigma(\delta) d\delta = J_{TIP} \tag{6}$$

Since the left hand side of Eq. 6 attains a maximum when $\sigma_i = \sigma_0$ (σ_0 = peak stress of the fiber crack bridging law) and $\delta_i = \delta_0$ (δ_0 = crack opening displacement at the peak stress of the fiber crack bridging law), the condition for SS cracking is guaranteed when the left hand size of Eq. 6 written for $\sigma_i = \sigma_0$ and $\delta_i = \delta_0$ is greater than J_{TIP} .

Note that, according to the proposed model, the development of a SS crack in each RVE is based on some crude assumptions: (i) SS crack propagation stage is neglected (i.e. the SS crack is assumed to instantly propagate to a length W); (ii) the sequence of crack initiation and propagation in different RVEs might be unrealistic (e.g. at a certain σ_i the SS condition of Eq. 6 might not be fulfilled); (iii) unstable crack propagation stage is neglected.

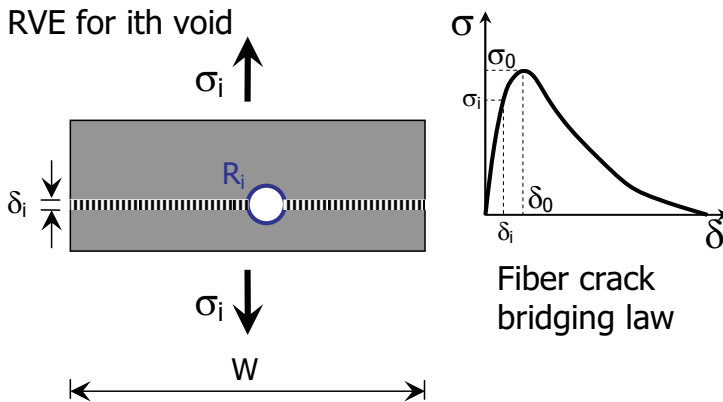


Figure 2. Fully developed SS crack in the i th RVE and relevant fiber crack bridging law.

Void-crack interaction. The stress field in the matrix, including that in the vicinity of voids, can be affected by the presence of already developed nearby SS cracks. Such an interaction between voids and cracks is due to the fact that in a SS crack the load is carried by the fibers crossing the crack surfaces. This load is transferred to the matrix near the crack through friction at the fiber-matrix interfaces. (Note that the load transfer from fiber to matrix dictates the minimum distance between adjacent multiple cracks in their saturation stage.) The distance over which the crack bridging load carried by the fibers is diffused in the matrix cannot exceed $L_f/2$, where L_f = fiber length (e.g. see Ref. [10]). Accordingly, in the present model this void-crack interaction is assumed to be relevant for $h_i < L_f/2$. Assuming a constant frictional strength at the fiber-matrix interfaces, the stress carried by the matrix linearly increases with the distance from the crack plane.

For crack initiation in the i th void a local tensile stress σ_i given by Eq. 5 is required. Now if there is an already developed SS crack in the $(i-1)$ th and/or $(i+1)$ th void, with the minimum distance h_{min} along the loading axis of the i th void from the developed SS crack(s) smaller than $L_f/2$, the remote tensile stress for crack initiation in the i th void has to be higher than σ_i because of the aforementioned fiber-to-matrix stress transfer phenomenon. Under the hypothesis of linear stress

diffusion, the remote tensile stress for crack initiation in the i th void σ_i^∞ can readily be calculated (for example $\sigma_i^\infty = \sigma_i (L_f / 2h_{\min})$).

Overall Stress-Strain Curves. The overall stress-strain curve of the ECC specimen under tensile loading can be predicted according to the present theoretical model. Since the load is applied under stress control, no unloading segments are detected in the curve. At the general k th load step, when the tensile stress σ_k is applied, the corresponding tensile strain ε_k can be calculated according to the following expression (noticing that at each step a new crack develops, so that at the k th step cracks already developed)

$$\varepsilon_k = \frac{\sigma_k}{E} + k \frac{\delta_k}{H} \quad (7)$$

where the contribution of elastic bulk deformation of the matrix and of opening displacement δ_k (for its meaning see insert in Fig. 2 where now the index i is to be regarded as k) of the SS cracks can be identified.

The ultimate tensile strain is attained for an applied stress equal to the peak stress of the fiber crack bridging law, σ_0 (the unstable final phase, characterized by a softening path in the stress-strain curve, is neglected), namely

$$\varepsilon_u = \frac{\sigma_0}{E} + N_a \frac{\delta_0}{H} \quad (8)$$

where N_a is the number of activated cracks/voids ($N_a \leq N_{TOT}$), i.e. the number of voids where a crack initiates and develops before reaching the failure load of the specimen.

Numerical Simulations and Comparison with Experiments

For the purpose of discussing the main characteristics of the proposed model, some numerical simulations are performed. Moreover, a comparison with some experimental results is performed to preliminarily validate the model.

The adopted input parameters for the model (in both numerical simulations and comparison with experiments) are as follows: $E = 20$ GPa; $f_{cr} = 4.5$ MPa; $J_{TTP} = 5$ J/m²; $\sigma_0 = 5.5$ MPa; $\delta_0 = 5$ μ m; $L_f = 12$ mm. The PDF of the void radius $p(R)$ is a Gaussian curve having a mean value of $R_{mean} = (R_{\min} + R_{\max})/2$ and a standard deviation s such that there is a 95% probability of occurrence in the range R_{\min} - R_{\max} ($R_{\min} = R_{mean} - 2s$ and $R_{\max} = R_{mean} + 2s$). The volume fraction of voids falling in the range R_{\min} - R_{\max} is taken as equal to 7% and is considered fixed in the simulation. As a result, the number of voids falls for a larger R_{mean} . The PDF of void spacing $p(h)$ is assumed to be uniform. Note that the condition of SS crack growth is fulfilled; as a matter of fact, assuming a linear piecewise fiber crack bridging law $\sigma(\delta)$, we have that the left hand of Eq. 6 for $\sigma_i = \sigma_0$ and $\delta_i = \delta_0$ is equal to 13.75 J/m², which is greater than the adopted value of J_{TTP} , as required.

In a series of simulations (see cases A to D in Table 1 below), the maximum radius of voids is kept constant and their radius range ΔR ($\Delta R = R_{\max} - R_{\min}$) is made to vary; for each range of variation of void radius, both cases with and without void-crack interaction are considered (see the overall tensile stress-strain curves in Fig. 3). Then a series of simulations (with void-crack interaction being considered) where ΔR is kept constant is performed (see cases E and F in Table 1

below). The ultimate tensile strain together with the total number of voids per unit surface and that of activated voids are summarized in Table 1.

Table 1. Summary of simulation results.

	Minimum radius, R_{min} [mm]	Maximum radius, R_{max} [mm]	No. of voids per $1m^2$	No. of activated voids per $1m^2$	Activated voids [%]	Threshold radius, R_{th} [mm]	Ultimate strain [%]	Void-crack interaction
A	0.25	2.50	22315	9733	43	0.9	4.89	w/o
B	0.50	2.50	13882	9784	70	0.9	4.92	w/o
C	1.00	2.50	8180	8180	100	-	4.12	w/o
D	2.00	2.50	4433	4433	100	-	2.24	w/o
A	0.25	2.50	22315	6560	29	N/A	3.31	w
B	0.50	2.50	13882	5256	37	N/A	2.66	w
C	1.00	2.50	8180	3524	43	N/A	1.79	w
D	2.00	2.50	4433	1912	43	N/A	0.98	w
E	0.25	1.25	55524	19489	35	0.7	9.77	w/o
F	1.50	2.50	5782	5782	100	-	2.92	w/o
E	0.25	1.25	55524	14015	25	N/A	7.04	w
F	1.50	2.50	5782	2482	43	N/A	1.27	w

As is clearly shown by the curves in Fig. 3, a significant influence of stress transfer from fiber to matrix (void-crack interaction) on tensile ductility is recorded. The upward kink in the predicted curves of Fig. 3 indicates that the voids which can be activated are exhausted well before reaching the peak stress σ_0 (the number of such voids is equal to 100% of the total number of voids for no void-crack interaction, see cases C, D in Table 1, and to 43% of the total number of voids for void-crack interaction, see cases C, D, F in Table 1). The other aspect which can be gathered from the analysis of Fig. 3 and Table 1 is the effect on tensile ductility of the range of variation of void radius. The ultimate strain is directly dependent on the number of activated cracks/voids N_a (see Eq. 8 and Table 1). Such a number N_a can easily be inferred in the case of no void-crack interaction from the range of variation of void radius. More in details, the number N_a is equal to the number of voids

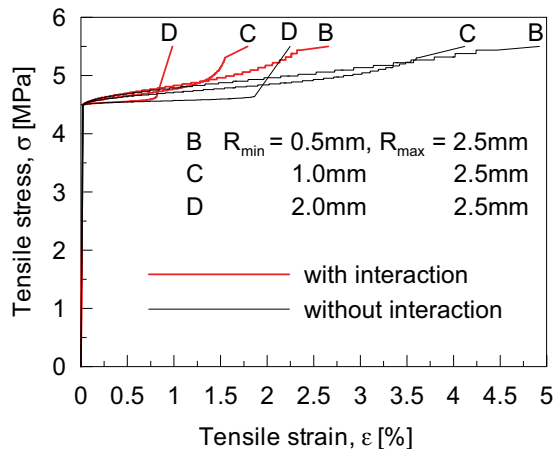


Figure 3. Predicted stress-strain curves: influence of void-crack interaction and of range of variation of void radius (see Table 1 for details of the results).

which, according to the function $n(R)$, falls in the range $R_{th}-R_{max}$, where R_{th} (see Table 1) is a threshold value of void radius below which no initiation and development of cracks occur (see e.g.

Ref. [6]). (Note that a threshold value of radius can be defined only if void-crack interaction is discarded. Note also that, see Table 1, the value of R_{th} might change as a result of a different value of a_0 obtained from Eq. 4 when R_{max} changes and f_{cr} is constant.) In Fig. 4 the PDF of void radius $p(R)$ and the distribution of void number $n(R)$ are reported for the cases B and C of Fig. 3. The higher number of activated cracks for case B (and in turn its higher ductility) as compared to that for case C is demonstrated by the larger area under the $n(R)$ curve in the interval R_{th} - R_{max} (note that, on the contrary, the area under the $p(R)$ curve in the same interval is smaller for case B with respect to case C).

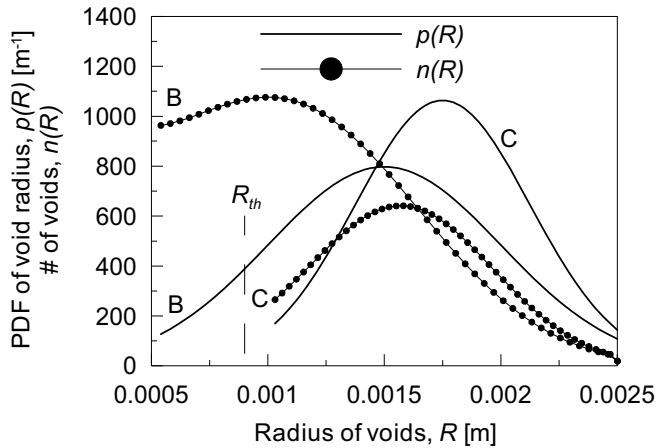


Figure 4. Probability density function of void radius $p(R)$ and distribution of void number $n(R)$ for $R_{min} = 0.5$ and 1mm , and $R_{max} = 2.5\text{mm}$.

Finally, a comparison with the experiments of Li & Wang [6] is given. In such experiments, two ECC mixes were tested under tensile loading: one mix contained natural voids (bubbles of entrapped air, with a volume fraction of about 7%) and the other mix contained in addition to natural voids a 7% volume fraction of artificial flaws with narrow size distribution (lightweight shale or plastic beads were used). The size of natural voids was in the typical range R_{min} - $R_{max} = 0.5$ - 2.5mm (a Gaussian PDF with 95% of occurrence in the range R_{min} - R_{max} is adopted), while the artificial flaws had a controlled size in the range R_{min} - $R_{max} = 1.75$ - 2.00mm (again a Gaussian PDF with 95% of occurrence in the range R_{min} - R_{max} is adopted), such that R_{min} is greater than an estimated value of R_{th} [6]. The PDF of void spacing $p(h)$ is assumed to be uniform in the present model. The predicted overall stress-strain curves are shown in Fig. 5. There is a good agreement with the trend of behavior of the experimental results (ultimate strain of about 1% for natural voids and of 3-4% for artificial voids), that is, the mix with artificial flaws exhibits a higher ductility than that of the mix with natural flaws only.

Conclusions

In the present paper, a simple micromechanical model is proposed to predict the overall tensile stress-strain curves of ECC. The material is treated as a chain of reference volume elements where each element contains a material flaw. Conditions for crack initiation at the flaw surface and for steady-state crack propagation within the reference volume element are defined. The model takes into account the randomness in size and in spatial distribution of material flaws. From the performed numerical simulations it is shown that, quite surprisingly, the tensile ductility might increase (the volume fraction of voids being the same) by enlarging the range of variation of void size or, alternatively keeping such a range of variation constant, by reducing the maximum void

size. This seems to indicate that the increase of tensile ductility due to the presence of artificial voids in the experimental tests of Li & Wang [6] is due to the higher number of activated cracks/voids which depends in turn on the higher volume fraction of voids. In other words, the mix design criterion of tailoring the distribution of void size so that its minimum value is greater than the threshold radius does not seem to guarantee alone to produce a higher tensile ductility in the ECC material, but further work would be required to substantiate this statement.

Further analyses into the numerical simulation of tensile behavior of ECC material are under way by using a 2D lattice model where the heterogeneity of the material (voids, etc.) is directly described in the model.

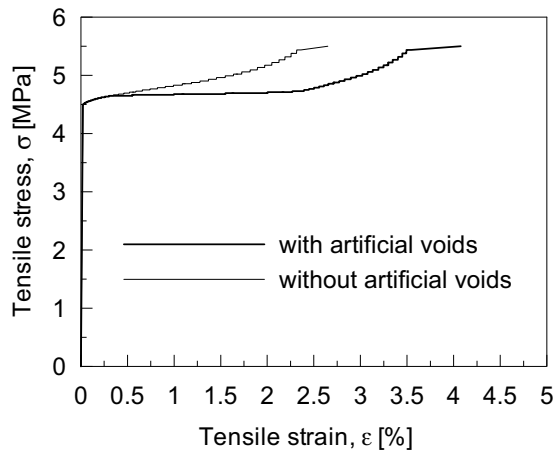


Figure 5. Simulation of experimental tests of Ref. [6].

Acknowledgments

AS would like to thank VCL for having hosted him during his visiting period at University of Michigan in Summer 2007, when the majority of the present work was carried out.

References

- [1] V.C. Li: JSCE J. Struct. Mechs & Earthquake Engng. Vol. 10 (1993), pp. 37-48
- [2] V.C. Li: *Concrete Construction Engineering Handbook*, edited by E. Nawy, chapter (CRC Press, 2008)
- [3] V.C. Li, S. Wang and C. Wu: ACI Mater. J. Vol. 98 (2001), pp. 483-492
- [4] D.B. Marshall and B.N. Cox: Mech. Mater. Vol. 7 (1988), pp. 127-133
- [5] S. Wang and V.C. Li, in: Proceedings of FRAMCOS-5, pp. 1005-1012 (2004)
- [6] V.C. Li and S. Wang: Probabilistic Engng Mechs. Vol. 21 (2006), pp. 201-206
- [7] P. Kabele: Engng Fract. Mechs. Vol. 74 (2007), pp. 194-209
- [8] P. Kabele and M. Stemberk, in: Proceeding of ICF11, Paper 4825 on CD ROM (2005)
- [9] H. Tada, P.C. Paris and G. Irwin: *The Stress Analysis of Cracks* (Paris Productions Incorporated and Del Research Corporation, St. Louis, MO, 1985)
- [10] H.C. Wu and V.C. Li: *J. Am. Ceram. Soc.* Vol. 75 (1992), pp. 3487-3489